Mathematical modelling and analysis of temperature effects in MEMS based bi-metallic cantilever for molecular biosensing applications

Miranji Katta[1,*], Sandanalakshmi R[2]

[1]*Dept. of Electronics and Communication Engineering, Sir C R Reddy College of Engineering, Eluru, Andhra Pradesh, India - 605014*

[1,2]*Dept. of Electronics and Communication Engineering, Puducherry Technological University, Pondicherry, India - 605014*

[*]*Corresponding author: miranji.katta@gmail.com*

Abstract

As Lab-on-Chip platforms with micro-and nano-dimensions evolve biosensors using miniaturized and high-sensitivity cantilevers are becoming more attractive. Although these sensors function in non-isothermal situations, computational mathematics generally ignores the temperature. Conversely, biosensor cannot be designed with a single-layered cantilever. Yet, in Nano-Electro-Mechanical-Systems, the influence of temperature is more likely to be dominant since the surface-to-volume ratio is higher. In the context of this conclusion, the mathematical modelling comprises temperature and the associated material attributes. This work presents a simple and direct analytical technique for analysing the control of bimetallic cantilevers with NEMS-based sensing and actuation mechanisms. Methodological techniques were used to develop and solve some well-known models of mathematical equations. Parametric analysis data is a major factor in the functioning of all of the other works studied. The findings of FEA comparisons and experiments reveal that the mathematical model's predictions are more than 20% correct.

Keywords: Actuation; bimetallic layers; bioMEMS; biosensors; temperature effects.

1. Introduction

As Lab-on-Chip platforms with micro-and nano-dimensions evolve, biosensors using miniaturized and high-sensitivity cantilevers are becoming more attractive. Although these sensors function in non-isothermal situations, computational mathematics generally ignores the temperature. Conversely, no biosensor can be designed with a single-layered cantilever. Yet, in Nano-Electro-Mechanical-Systems, the micro-electro-mechanical systems (MEMS) have recently enabled the medical sector to develop a new generation of chemical and biological sensors. When it comes to biological sensing, NEMS and the sensors and actuators that go with it are becoming important and it is possible to build sensing systems using micro-and nanoscale parts. The outcome of such systems are more reliable, faster, and accurate (Gupta *et al.*, 2016), (Vasan, Doraiswami and Pecht,

2011). Microsensors and actuators based on silicon were the standards in the early 1990s. MEMS devices have been increasingly popular since they emerged to develop IC manufacturing technologies. It has been claimed that a wide range of MEMS-based sensors may be used in a wide range of scientific fields, including biochemicals, microfluidics, and aeronautical and optical studies. Micro bridges and cantilevers, two components of MEMS and NEMS, have several medical applications. Most intelligent systems are likely to include core structures with numerous layers (Mohd Ghazali *et al.*, 2020). It has only been that novel actuation techniques have evolved in the past few years. An actuation mechanism called the bimetallic effect may be of interest if you wish to regulate displacement in response to temperature changes (Navakul *et al.*, 2017). A NEMS cantilever's deflected free-end characteristic and force relationship are explored here to determine the cantilever's temperature change. To create actuation, the free end of the cantilever must move in a perpendicular direction(Ali *et al.*, 2017). According to Figure 1, a bimetallic cantilever has a typical temperature influence on molecules.

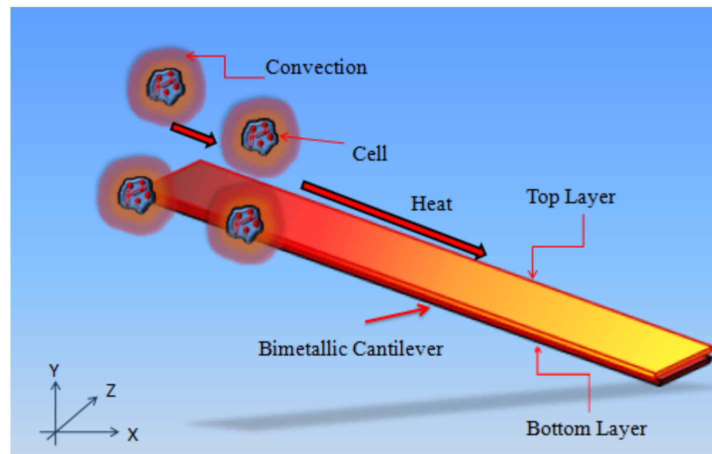

Fig. 1. Temperature effect on bimetallic cantilever with respect to molecular biosensing

1.1 Temperature Effects on Sensing Methods

Many sensing technologies, such as tuneable capacitors have been developed for micro to nano sensing applications (Kouravand, 2011). There are several sources of information on sensing and actuation, with the most widely employed techniques being chemical, optical, thermal, mechanical, piezoresistive, capacitive, piezoelectric, resonant, magnetic, electrostatic, and so on (Cote, Lec & Pishko, 2003), (Fu *et al.*, 2007), (Saylan *et al.*, 2019). This research presents a series of unique integrated capacitive sensing and actuation technologies based on nanostructures. Capacitance fluctuations caused by the deflection of bimetallic cantilevers loaded by linear or nonlinear electrostatic forces and thermal bending forces are used in sensors and actuators (Vineetha *et al.*, 2018), (Hegner & Arntz, 2003). The static behaviour of nano cantilever beams was also investigated (Katta *et al.*, 2020).

Thermal noise is produced when a microcantilever is in thermal equilibrium with its surroundings (vibration caused by thermal agitation). Due to energy dissipation, the mechanical energy stored in a microcantilever is wasted as heat (Khaleel & Hashim, 2020). Random excitation is caused by the multiple microscopic degrees of freedom in a microcantilevers environment. The statistical mechanics "fluctuation-dissipation theorem" captures the relationship between energy dissipation and random thermal excitation(Nordström *et al.*, 2008), (Yu-Jie Huang *et al.*, 2013). Consequently, lower mechanical Q results in a more noticeable noise force. equation. 1 demonstrates the "equi-partition theory" to obtain the mean square vibration amplitude for a certain oscillation mode at temperature T.

$$\frac{1}{2}k_B T = \frac{1}{2}k_B z^2 \tag{1}$$

When the microcantilevers deflection is measured, k_B is the Boltzmann constant, k is its stiffness, and z is its displacement. The spectral density S_F $(4k_B TB/\omega_o Q$ and the force noise (F) in a bandwidth (B) are given by equation. 2 if the noise spectrum is assumed to be white (i.e., frequency-independent) (Kouravand, 2011b).

$$F_{min} = \sqrt{\frac{4k_B TB}{\omega_o Q}} \tag{2}$$

There is a natural cantilever frequency, f_0, equal to $2f_0$. equation. 3 may represent a minor measurable force on a rectangular cantilever (Neethu & Suja, 2016).

$$F_{min} = \left(\frac{wt^2}{LQ}\right)^{\frac{1}{2}} (k_B TB)^{\frac{1}{2}} \left(E_\rho\right)^{\frac{1}{2}} \tag{3}$$

Its width (w), thickness (t), length (L), E (Yang's modulus), and density (F) are all measured in units of density. In the same way, the mean square root deflection is obtained by equation. 4, (Vineetha *et al.*, 2018).

$$z_{rms} = \left(\frac{kT}{k_B}\right)^{\frac{1}{2}} = \left(\frac{2kT}{wE}\right)^{\frac{1}{2}} \left(\frac{L^3}{t^3}\right)^{\frac{1}{2}} \tag{4}$$

Although equation. 3 and 4 may be utilised to design the sensitivity of microcantilevers, it is clear that very high-quality factors are required for ultrasensitive devices.

1.2 Effect on material properties

The temperature has a significant impact on the characteristics of microcantilever (Neethu & Suja ,2016 and Mathur *et al*., 2016), (Rosen & Gurman, 2010). For example, elastic modulus decreases

with increasing temperature. For the high-temperature limit, the elastic modulus of silicon has been modelled semi empirically using equation. 5.

$$E(T) = E_0 - BT\, exp(-\frac{T_o}{T}) \tag{5}$$

Where E_0 is Young's modulus at absolute zero degrees Celsius. Temperature-independent constants B > 0 and T_o > 0 are aluminium trioxide (Al_2O_3), E_0 is around 4.6×10^{12} dyn/cm^2, B is 4.41×10^8 dyn/cm^2, and T_0 is 373°K. Over a wide range of temperatures, the frequency shift of silicon microcantilevers and changes in the Q-factor have been examined (Chen & Feng, 2011 and Kim *et al.*, 2019).

1.3 Effect on Geometry

The geometry of a microcantilever is also affected by temperature, with a rise in temperature being correlated to an increase in dimensions via a metric known as the coefficient of thermal expansion (CTE). A polymer's thermal expansion is in the range of 50 –100 parts per million (ppm) per degree Celsius, whereas silicon is 3.2ppm/^{o}C. As can be seen from the explanation presented here, the microcantilevers calibration and operation must be accomplished at the same temperature and within extremely tight tolerances. Differential measurements using coated and uncoated microcantilevers must be carried out without temperature control (Boisen & Thundat, 2009). Perhaps the first time, we used computational modelling to conduct an in-depth and systematic investigation into the influence of Au layer coverage and thickness on the thermo-electro-mechanical characteristics of the sensor. The prediction model is tested by comparing theoretical values to experimental data given in the literature.

2. Literature Survey

In a recent work, researchers discovered that resistive/Joule heating of dc-biased piezoresistors has a considerable impact on the performance of this double piezo - resistive micro/nano cantilevered sensors (Wee *et al*., 2005). (Lee *et al*., 2015). Furthermore, it was demonstrated that self-heating induced cantilever deflection, resulting by a variation in the thermal coefficient of expansion (TCE) level in a hybrid cantilever. It is the most significant contribution to thermal drift in sensor output. As a result, the present research will be helpful in answering the following questions: (i) to achieve insight into the effect of multi-layer due to the large TCE, which contributes significantly to TCE stimulated deflection and therefore thermal drift inaccuracy (sensor reliability); and (ii) to optimize not only measurement reliability by diminishing thermal drift but also sensor performance in terms of both electrical and biological sensitivity by optimization the coverage and thickness of each layer.(Wadas *et al*., 2017; Rao & Wootla, 2007; Miranji & Sandanalakshmi R, 2020a; Katta *et al.,* 2021).

This work uses a finite element method (FEM) based solver owing to the sensors complicated composite construction and multiphysics environment. Even though mathematical models are employed to forecast the cantilever deflection profile, resonant frequency, and TCE induced deflection. Aside from the reasons stated above, the inability of simplified models to predict complex multi-morph deflection, the geometrical influence of the Au patch on the cantilever platform, and the abrogation of the coverage effect of Au on TCE deflection all contribute to the accuracy of computer-based computation model.

2.1 Experimental validation

Computational findings are compared with experimental data from different devices described in the literature to validate the modeling method used in this study. To compare our modeling method, researcher's modeled devices documented in the literature with the same shape and applied thermal, electrical, and mechanical boundary conditions to examine their properties. Table 1 summarizes the comparison of modeling techniques with experimentally reported data.

Table 1. Comparison of modeling techniques with experimentally reported data.

Reference	Simulation Results	Experimental Results	% Change
	Relative change in Nominal Resistance($\Delta \boldsymbol{R}/\boldsymbol{R}$)		
Zhou *et al*., 2009	1.81×10^{-3}	1.1×10^{-3}	6.45
Loui *et al*., 2008	0.65×10^{-4}	0.6×10^{-4}	8.33
	Input power-10mW		
Lee *et al*., 2007	209°C	200.34°C	4.32
	Non-Identical TCE residual deflection		
Zhou *et al*.,2009	84.15nm	79.20nm	6.25

According to Lee *et al*., (2015) modeled and examined the device's temperature profile and maximum cantilever temperature (T_{max}) to compare thermal modeling approaches. The cantilever's maximum temperature has been taken into account in our calculations. The maximum temperature

of the modeled device is 209ºC at a power level of 10mW. However, the device's recorded temperature is 200.34ºC, resulting in a 4.32 percent inaccuracy. Furthermore, we simulated a silicon dioxide cantilever sensor described by Zhou (Zhou *et al.*, 2009) to compare the cantilever's thermo-mechanical response (Z/Z|TCE). According to the results, the magnitude of Z/Z|TCE for the modeled device is 84.15nm. For the identical device, the reported value of Z/Z|TCE is 79.20 nm, which is 6.25 percent lower than the modeled device. Both point loading (R/R|p) and surface stress loading (R/S) are used to verify the electro-mechanical modeling technique. We simulated the device published by Loui *et al*. (Li *et al.*, 2008) to compare electro-mechanical response, i.e., ΔR/R input due to point loading. The magnitude of ΔR/R for the modeled device (0.64×10^{-4}) and the experimentally reported value (0.6×10^{-4}) differ by 6.66 percent at an endpoint tip deflection of 1.7mm. A 4.54% deviation in the magnitude of R/R|s produced by modeling the constructed device was found in the results. There is a discrepancy between the simulated device's R/R|s and the stated value of 1.15×10^{-3}m/N. Because of this, the discrepancy between the model findings and the presented experimental data is considered reasonable.

3. Mathematical Modelling

Figure. 2(a) shows the schematic of the bi-metallic cantilever geometry of the nano actuator with length ℓ, thickness t, width w, and elasticity modulus E. In contrast, bottom layer parameters are indicated with subscript 1, and top layer parameters are indicated with subscript 2. In the designed model, two metallic layers are sandwiched and assumed to be identical in length. Such an arrangement is suitable for providing the maximum force (assuming all other parameters are constant). All other parameters may be dissimilar and denoted with indices 1 and 2, respectively. Let us suppose that where is the coefficient of thermal expansion (see figure 2). Usually, bimetallic nanoactuators use metals deposited onto silicon and conform to this assumption. An embedded heating resistor assumes a homogeneous thermal distribution encircling the cantilever. "X" indicates the length, and "Z" indicates the cross-section at the origin. A beam deflection w(x) alongside the x-axis is presented in figure.2 (c).

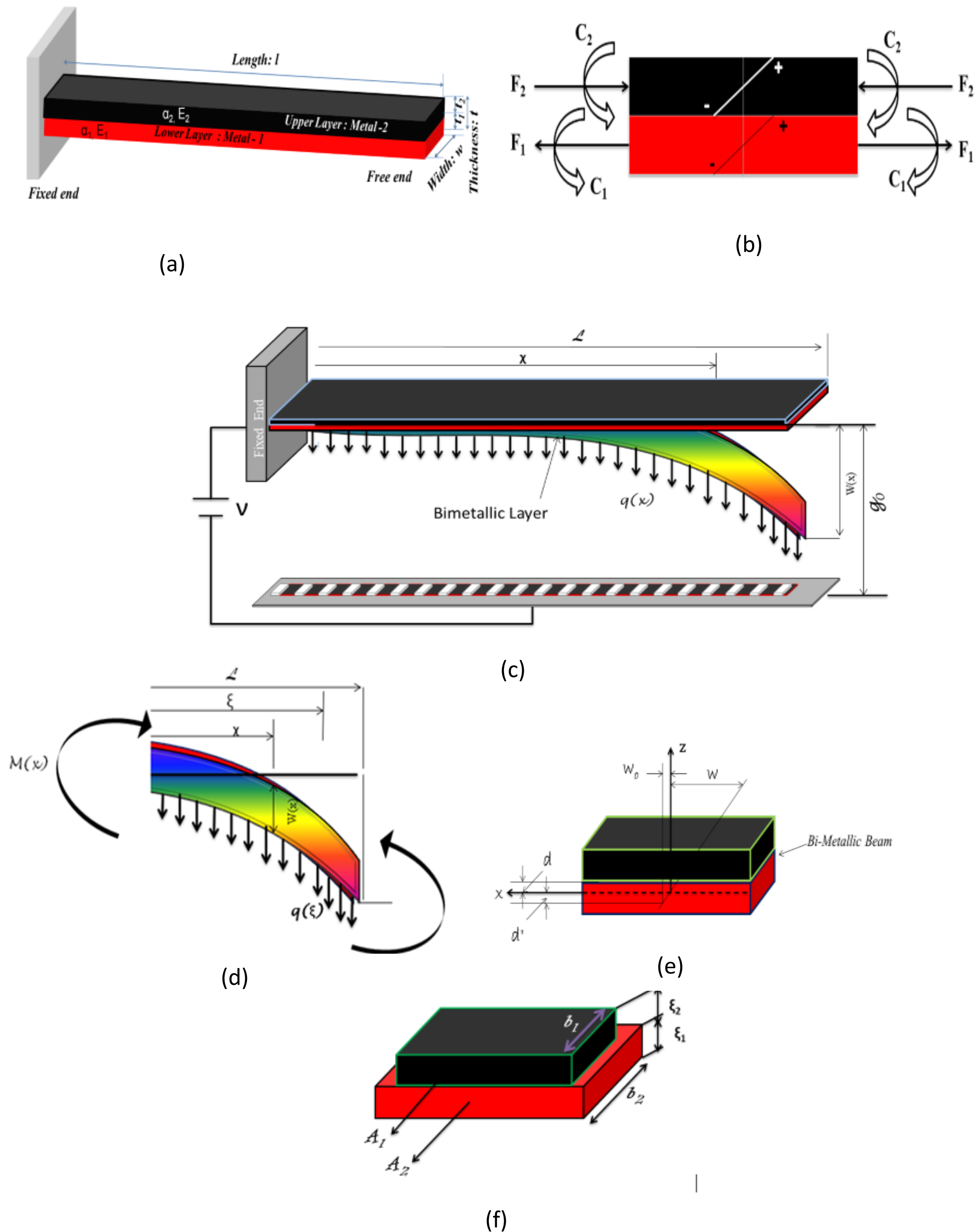

Fig. 2. The cross-sectional area of bimetallic cantilever (a) Forces acting on the cross-section of the segment along the course of the cantilever (b) Moments acting on the cross-section of the segment along its length (c) Schematic of Electrostatic cantilever beam (d) Deflection due to electrostatic force alongside the beam (e) An constituent of bi-layered cantilever beam towards x and z directions (f) Slippage between bi metallic layers.

On the sandwiched beam, segments cross-section is shown in Figure 2(b) as force and moment imposed by increasing temperature. There are tensile and compressive forces F_1, F_2, coupled by C_1 and C_2 across the sections of material 1 and 2, which result in different internal stresses. These forces must be in equilibrium over any cross-section of the beam(Miranji Katta & Sandanalakshmi R, 2020) i.e.

$$F_1 = F_2 = F \tag{6}$$

$$\frac{F(t_1 + t_2)}{2} = C_1 + C_2 \tag{7}$$

According to beam Theory

$$C_1 = \frac{E_1 I_1}{r} \qquad C_2 = \frac{E_2 I_2}{r} \tag{8}$$

Where $\boldsymbol{E}$-Young's modulus and $\boldsymbol{I}$ - moment of inertia, $\boldsymbol{r}$- radius of beam curvature. By using equation (3), (2) can be reduced to

$$\frac{F(t_1 + t_2)}{2} = \frac{E_1 I_1}{r} + \frac{E_2 I_2}{r} \tag{9}$$

Above equation has two unknown parameters $\boldsymbol{F}$ and $\boldsymbol{r}$, hence one more equation is needed to relate these parameters. At the inner surface, ordinary strain of two sandwiched layers are same, therefore

$$\alpha_1 \Delta T + \frac{F}{E_1 t_1 b_1} + \frac{t_1}{2r} = \alpha_2 \Delta T - \frac{F}{E_2 t_2 b_2} - \frac{t_2}{2r} \tag{10}$$

Here ΔT is the change in temperature and *t, w* are thickness and width of the cantilever beam, $I_1$and I_2 are $\frac{b_1 t_1^3}{12}$, $\frac{b_2 t_2^3}{12}$ respectively.

By solving the above equation for beam curvature $k = \frac{1}{r}$ is

$$\boldsymbol{k = \frac{1}{r} = \frac{6b_1 b_2 t_1 t_2 E_1 E_2 (t_1 + t_2)(\alpha_2 - \alpha_1)\Delta T}{(b_1 E_1 t_1^2)^2 + (b_2 E_2 t_2^2)^2 + 2b_1 b_2 t_1 t_2 E_1 E_2 (2t_1^2 + 3t_1 t_2 + 2t_2^2)}} \tag{11}$$

There are many bimetallic cantilever-based actuators with numerical (nearly non-zero) tip deflections (Chu *et al.,* 1993). In particular NEMS based cantilevers, due to their small dimensions and thickness, the temperature effects are more dominant, and the curvature is existed because of residual stress in the thin-film materials (Mathur *et al.,* 2016). Two basic assumptions are made in

equation (11), which states a linear distribution of strain over the beam thickness and that two sandwiched materials are perfectly bonded at their edges. The equation (11) can represent changes in curvature with temperature in a bimetallic cantilever with non-zero deformation. The curvature derived in equation (12) is different from the below equation of previous publication (Chen & Feng, 2011 and Chun-Hao & Chen, 2009) and is being used in the field of nanomechanics

$$K = \frac{1.5(t_1 + t_2)\Delta\alpha\Delta T}{1.75(t_1 + t_2)^2 - 2t_1 t_2 + (E_1 b_1 t_1^3/E_2 b_2 t_2) + (E_2 b_2 t_2^3/E_1 b_1 t_1)} \quad (12)$$

In addition to tip deflection, the force generated at the bimetallic cantilever's edge (free end) is also studied here. A bimetallic cantilever can deflect as temperatures vary due to the material’s temperature coefficient. Therefore, it is necessary to provide an external counter force **Feq** to the beam to avoid the bi-metallic effect to regulate the cantilever's tip at a fixed point. When a cantilever is loaded at the end, its deflection is given by beam theory as (Chen & Feng, 2011), (Zhou *et al.*, 2009).

$$F_{eq} = 3EId/l^3 \quad (13)$$

Here employed the transformed-section technique (Kooser *et al.,* 2003 and Passian & Thundat, 2008) to calculate the composite cantilever EI's flexural stiffness. An axis of neutral rotation doesn't need to be centred on a bimetallic beam's cross-section and cross-sectional dimensions. When the cantilever is subjected to thermal strain, its free end has constant curvature, resulting in a deflection of the magnitude (Yanagida *et al.,* 2017):

$$d = k\, l^2/2 \quad (14)$$

For $l \ll r$.

Tip force and temperature can be converted to each other with ease if tip deflection is determined as a function of input power or temperature using equation (8). Figure 3(a) shows both the free end bending and the force generated when the electric input power is increased. As shown in Figure 3, a deflection occurs without a tip (b). Analyzing the acquired research results, we compare them to the findings of the finite element method. Figure 4 depicts the cantilever tip deflection as a function of temperature change using a 3-D finite element analysis simulation model.

The cantilever deflection in the second instance is caused by temperature variations and the electrostatic force applied along the beam, as shown in Figure (2a). Figure 2(b) shows that the bending moment is expressed as (Yang *et al.*, 2016):

$$\mathrm{M(x)} = \int_x^{\ell} q(\xi)(\xi - x)d\xi \quad (15)$$

Here $\boldsymbol{q(\xi)}$ is electrostatic force in unit lenth is obtained from the below equation(Chu *et al.,* 1993)

$$q(\xi) = \frac{\varepsilon_o V_b^2 w}{2(g_o - w(\xi))^2} \tag{16}$$

Here $\boldsymbol{\varepsilon_o}$, $\boldsymbol{v_b}$, w, $\boldsymbol{g_o}$, $\boldsymbol{w(\xi)}$, are air permittivity, bias voltage applied to beam, width of the bi-metallic cantilever beam, preliminary gap and beam deflection respectively. As per the above equation deflection of the beam is nonlinear. From the above two equations, the correlation between deflection of bi-metallic cantilever at a given temperature can be expressed as

$$\frac{d^2w}{dx^2} = \frac{12n(\alpha_1 - \alpha_2)\Delta T}{h(n^2 + 14n + 1)} + \frac{6(1+n)\varepsilon_o V_b^2}{E_1(n^2 + 14n + 1)h^3} \int_x^l \frac{(\xi - x)}{\left(g_o - w(\xi)\right)^2}\, d\xi \tag{17}$$

When the applied voltage or temperature variations are increased, linearizing the above equation concerning w may cause significant errors. This is because "ω" has a large value relative to the initial gap. As a result, it is recommended that the applied voltage and temperature be progressively raised (Mukhopadhyay *et al.*, 2005 and Kouravand *et al.,* 2011). It is linearized by utilizing the Step-by-Step Linearization Method (SSLM) and generates a linear differential equation that is solved by using the Finite Difference Method (FDM).

4. Results and Discussions

The dimensional parameters of the cantilevers are α_1=3.2x10^{-6}, α_2=1.85x10^{-5}, E_1=150GPa, E_2=60GPa, L_1 = 400nm, L_2 = 350nm, W_1 = 120nm, W_2 = 100nm, t_1=18nm, t_2=25nm, they are the same parameters used in [2] for the fabrication and measurement of the devices (see Figure. 3(b)). Using (11), the estimated tip deflection is just 6% off from what the FEA predicted. The computed tip deflection using (12) is clearly incorrect. The nanofabricated bimetallic cantilevers used in this study were tested in two different ways. Researchers assess the bimetallic cantilever temperature anomaly in the atmosphere with respect to electrical power input during the first experiment. The cantilever edge deformation in the air is determined, in the second experiment as a function of electrical input power.

The following simulation results with COMSOL multiphysics in the static and dynamic environment, parametric sweep variable as temperature (T) shows different resonance frequencies (f_o). For the above dimensional parameters, variable temperature 25, 40, 55, 70, 85, 100 in ^{O}C shows various resonance frequencies from figure 3(a)-(f). Here double layers of cantilever beam simulated individually for the analysis of TCE effect on deflection and resonance levels.

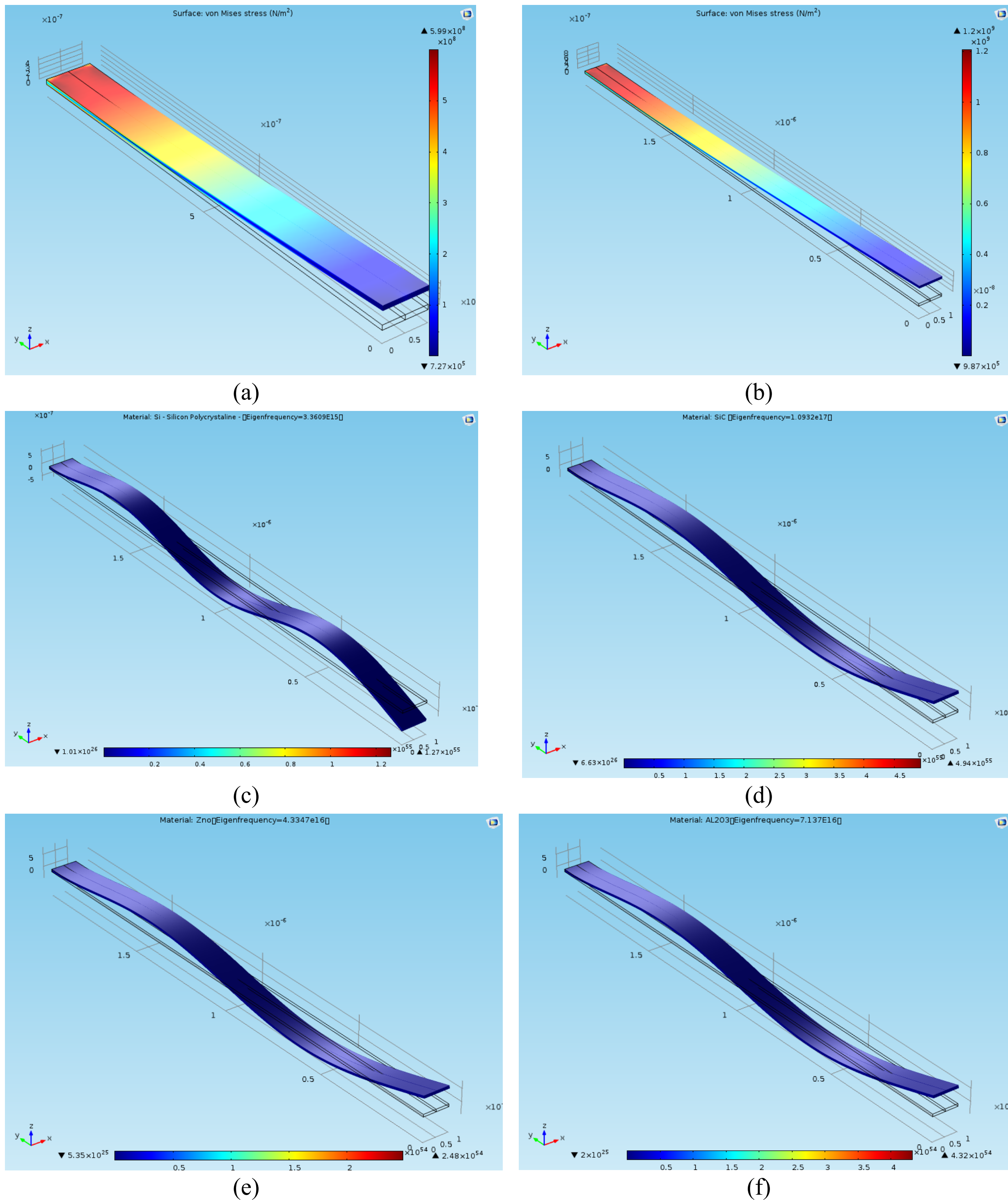

Fig. 3. COMSOL-Simulation results of cantilever beam under static and dynamic analysis with identical temperature range (a) Deflections capability of top layer (b) Deflections capability of bottom layer (c) & (d). Resonance frequency change in top layer (e) & (f) Resonance frequency change in bottom layer

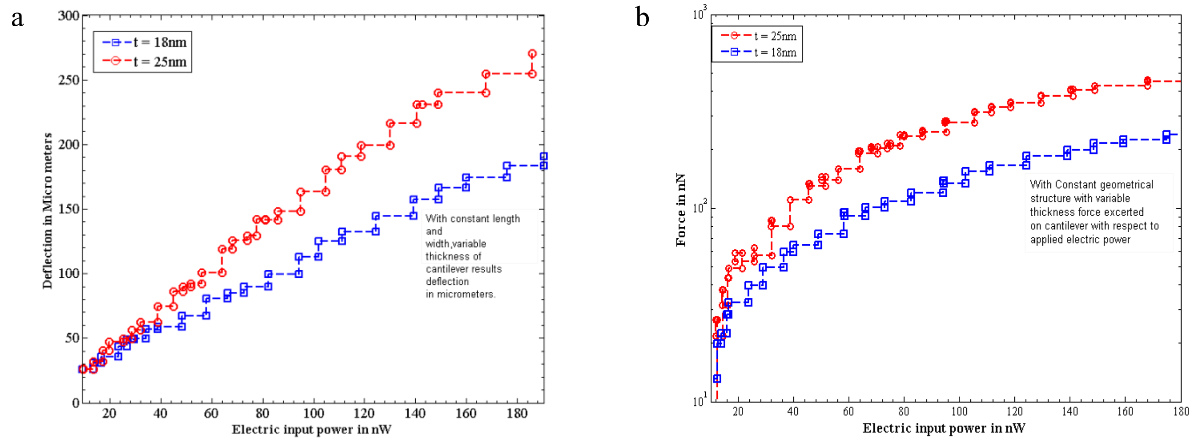

Fig. 4. Response of cantilever beam in air medium (a) Tip deflection with electric power input (b) Force developed due to electric input power.

The cantilever's temperature-dependent tip deflection may be computed by adding the findings from these different experiments. For the bimetallic cantilevers according to Chu *et al.,* (2009), the edge deformation is not zero in the presence of residual stresses. The ambient temperature required to compensate for the pre-set tip deflection may be used to accommodate for the starting curvature. The estimated tip deflection based on equations (12) and (17) are shown in Table 2 precisely, the developed model here provides more accurate results.

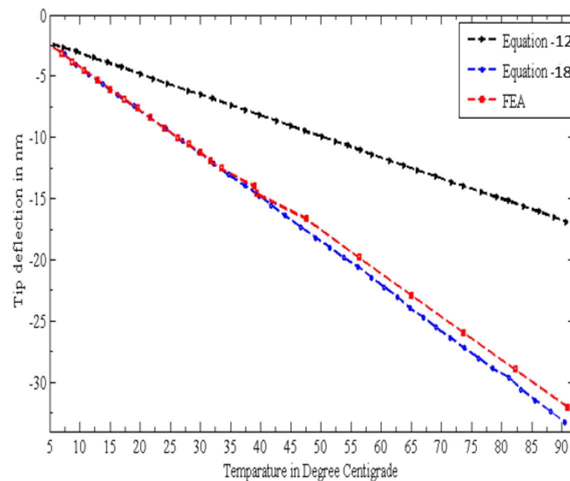

Fig. 5. Estimated edge deformation using (12) and (18) and finite-element analysis

Table 2. Comparison of edge deformation calculated from (7) and (8) with Experimental results

Measured Temperature in (°C)	Measured Tip Deflection in nm	Deflection Calculated using (6)	Deflection Calculated using (7)
25	680	654.78	382.15
40	470	448.92	225.48
55	368	354.68	124.32
70	175	158.14	79.56
85	128	112.25	59.46
90	68	64.78	31.25

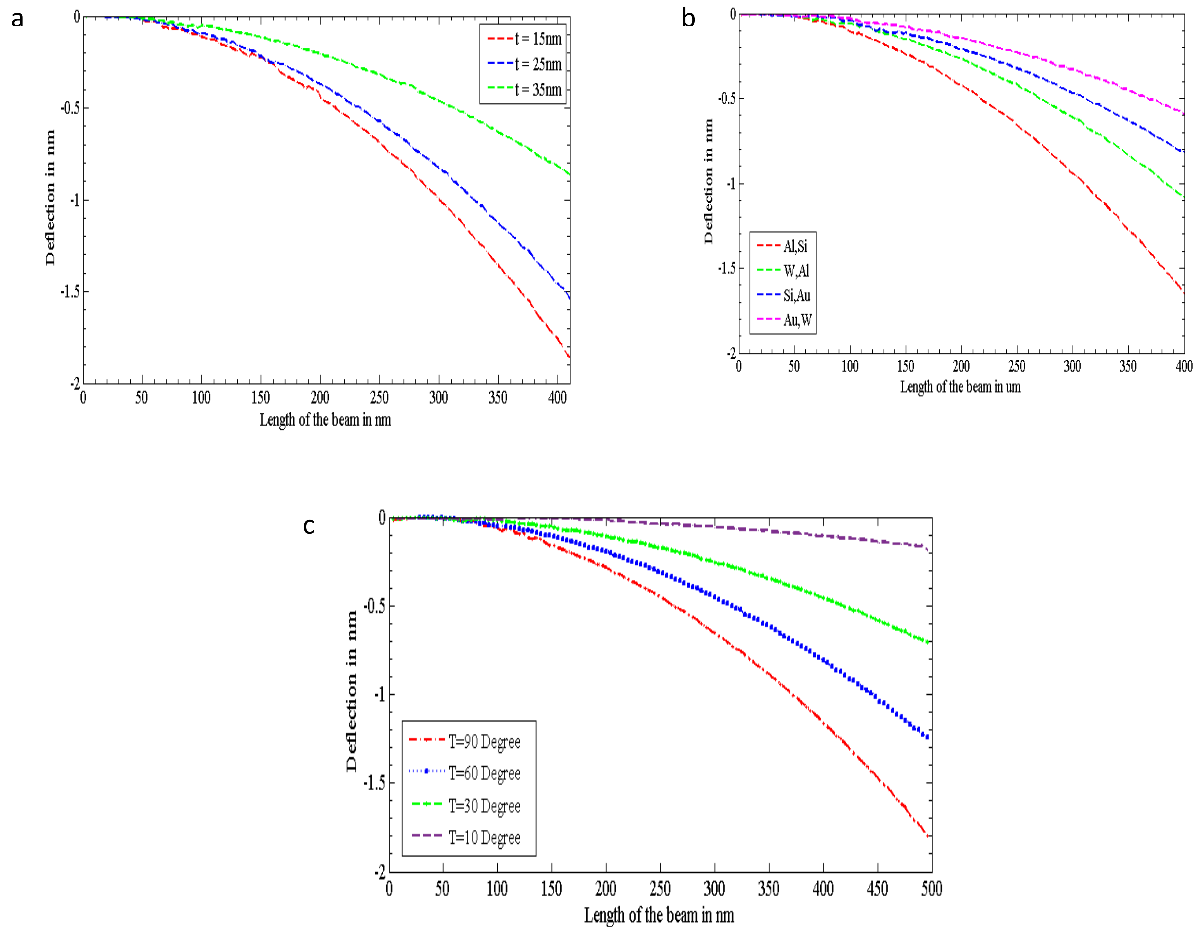

Fig.6. The influence of composite material arrangement on bimetallic beam deflection (a) Reverse relationship between beam deflection and a bimetallic layer thickness (b) Effect of material arrangements on beam deflection in a second model. (c) Deflection of the bimetallic cantilever with respect to temperature for the second model.

Analyzing a bimetallic cantilever nano actuator edge deflection and force using a simple methodical form is presented. Experimental results and comparison with finite element simulation are used to verify the model's validity. Analytical results of the model presented have an accuracy of at least 20% from ccomparison of tip deflection computed from (12) and (18) with experimental results obtained.

When the temperature does not alter, the bending of a beam is solely dependent on the electric potential applied. Figure 6(c) shows the deflection of the beam structure as the temperature increases. The bias voltage may be changed to adjust the lateral deformation. For a statistical approach, the deformation of a cantilever is calculated using the Finite Difference Method (FDM). Depending on the system's geometrical and material characteristics, simulation output results may vary significantly. The deflections of cantilever beams depend on the type of material and geometrical properties that have been used. For the second model, with a temperature increase of 50ºC and a bias voltage of 5 volts, the results are given in Figures 6(a) and (b). Bimetallic cantilever beams were shown in Figure. 3 to show the various impacts of material configurations on displacement. Increasing the variance in thermal expansion coefficients (CTE) between layers increases the suggested model's responsiveness. To further illustrate this, if the thickness of each layer in a bimetallic cantilever beam is increased, the flexural deformation decreases (see Figure. 6 (a)). Therefore, the model's sensitivity to beam deflection has an inverse relationship to the thickness of the bimetallic layer.

5. Conclusion

In this paper, a mathematically modeled nano-electro-mechanical cantilever is investigated. Models are composed of governing equations obtained and solved numerically and analytically. Numerical findings show that using the appropriate materials and geometric characteristics may increase sensitivity. From the simulation findings, the difference between the coefficients of thermal expansion (CTE) of layers increases as the cantilever's length increases. Improvement in cantilever beam deflection when the layer thickness is minimized.

In contrast, this approach has many limitations, which can potentially lead to a muddled system. This limitation arises from the need to select the voltage such that the pull-in phenomenon is avoided when selecting the voltage. Compared with electrostatically actuated thermal actuators, the electro-thermal actuating mechanism has several advantages, such as avoiding static charges on the plates, improving the tuning reliability, and requiring lower driving voltages. Considering these factors as a whole could be necessary for a particular design of MEMS. Moreover, their use at various temperatures is affected by dimensions, materials, the level of sensitivity required, and environmental factors.

ACKNOWLEDGEMENTS

I would like to express my sincere thanks to the Nanosniff technologies center and the NMR Spectroscopy for Pharma and Biotech Research center, both of which are located at the Indian

Institute of Technology, Mumbai, for providing the necessary technical support and valuable guidance during the experimental work.

References

Ali, J. *et al.* (2017) 'Biosensors: Their Fundamentals, Designs, Types and Most Recent Impactful Applications: A Review', *Journal of Biosensors & Bioelectronics*, 08(01). doi:10.4172/2155-6210.1000235.

Boisen, A. and Thundat, T. (2009) 'Design & fabrication of cantilever array biosensors', *Materials Today*, 12(9), pp. 32–38. doi:10.1016/S1369-7021(09)70249-4.

Chen, S.H. and Feng, B. (2011a) 'Size effect in micro-scale cantilever beam bending', *Acta Mechanica*, 219(3–4), pp. 291–307. doi:10.1007/s00707-011-0461-7.

Chu, W.H.M., Ehran M, Robert LM. (1993) *Analysis of tip deflection and force of a bimetallic cantilever microactuator. JM icromeec Microeng*, *3*, pp.4-7.

Chun-Hao Chen *et al.* (2009) 'A Wireless Bio-MEMS Sensor for C-Reactive Protein Detection Based on Nanomechanics', *IEEE Transactions on Biomedical Engineering*, 56(2), pp. 462–470. doi:10.1109/TBME.2008.2003262.

Cote, G.L., Lec, R.M. and Pishko, M.V. (2003) 'Emerging biomedical sensing technologies and their applications', *IEEE Sensors Journal*, 3(3), pp. 251–266. doi:10.1109/JSEN.2003.814656.

Finot, E., Passian, A. and Thundat, T. (2008) 'Measurement of Mechanical Properties of Cantilever Shaped Materials', *Sensors*, 8(5), pp. 3497–3541. doi:10.3390/s8053497.

Fu, L. *et al.* (2007) 'Magnetostrictive Microcantilever as an Advanced Transducer for Biosensors', *Sensors*, 7(11), pp. 2929–2941. doi:10.3390/S7112929.

Gupta, S. *et al.* (2016) 'Lab-on-Chip Technology: A Review on Design Trends and Future Scope in Biomedical Applications', *International Journal of Bio-Science and Bio-Technology*, 8(5), pp. 311–322. doi:10.14257/ijbsbt.2016.8.5.28.

Hegner, M. and Arntz, Y. (2003) 'Advanced Biosensing Using Micromechanical Cantilever Arrays', in Braga, P. C. and Ricci, D., *Atomic Force Microscopy*. New Jersey: Humana Press, pp. 39–50. doi:10.1385/1-59259-647-9:39.

Katta, M. *et al.* (2020) 'Static and Dynamic Analysis of Carbon Nano Tube Cantilever for Nano Electro Mechanical Systems Based Applications', *Journal of Computational and Theoretical Nanoscience*, 17(5), pp. 2151–2156. doi:10.1166/jctn.2020.8862.

Katta, M. and Lavanya, K. (2021) 'simulation approach to design high sensitive nems based sensor for molecular bio- sensing applications', *Clinical Medicine*, 08(03), p. 9.

Khaleel, R.S. and Hashim, M.S., 2020. Fabrication of ZnO sensor to measure pressure, humidity and sense gases at room temperature by using rapid breakdown anodization method. *Kuwait Journal of Science*, *47*(1).

Kim, J.H. *et al.* (2019) 'Development of peptide biosensor for the detection of dengue fever biomarker, nonstructural 1', *PLOS ONE*. Edited by S. D'Auria, 14(9), p. e0222144. doi:10.1371/journal.pone.0222144.

Kooser, A. (2003) 'Investigation of the antigen antibody reaction between anti-bovine serum albumin (a-BSA) and bovine serum albumin (BSA) using piezoresistive microcantilever based sensors', *Biosensors and Bioelectronics*, 19(5), pp. 503–508. doi:10.1016/S0956-5663(03)00221-5.

Kouravand, S. (2011a) 'Design and modeling of some sensing and actuating mechanisms for MEMS applications', *Applied Mathematical Modelling*, 35(10), pp. 5173–5181. doi:10.1016/j.apm.2011.04.015.

Lee, J. *et al.* (2015) 'Enhanced performance of an innovative dengue IgG/IgM rapid diagnostic test using an anti-dengue EDI monoclonal antibody and dengue virus antigen', *Scientific Reports*, 5(1), p. 18077. doi:10.1038/srep18077.

Li, X. *et al.* (2009) 'Integrated MEMS/NEMS Resonant Cantilevers for Ultrasensitive Biological Detection', *Journal of Sensors*, 2009, pp. 1–10. doi:10.1155/2009/637874.

Mathur, H., Agarwal, V. and Sengar, K. (2017) 'Finite Element Analysis of MEMS based Piezoresistive Diamond Thin Film Cantilever Pressure Sensor', 04(02), p. 5.

Miranji Katta and Sandanalakshmi R (2020a) 'Geometrical Sensitivity Analysis of Bio-Nano Electro Mechanical Systems Using FEM Analysis For Disease Detection', *Bioscience Biotechnology Research Communications*, 13(2), pp. 49–58.

Mohd Ghazali, F.A. *et al.* (2020) 'MEMS actuators for biomedical applications: a review', *Journal of Micromechanics and Microengineering*, 30(7), p. 073001. doi:10.1088/1361-6439/ab8832.

Mukhopadhyay, R. *et al.* (2005) 'Cantilever Sensor for Nanomechanical Detection of Specific Protein Conformations', *Nano Letters*, 5(12), pp. 2385–2388. doi:10.1021/nl051449z.

Navakul, K. *et al.* (2017) ‘A novel method for dengue virus detection and antibody screening using a graphene-polymer based electrochemical biosensor’, *Nanomedicine: Nanotechnology, Biology and Medicine*, 13(2), pp. 549–557. doi:10.1016/j.nano.2016.08.009.

Neethu, K. and Suja, K.J. (2016) ‘Sensitivity Analysis of Rectangular Microcantilever Structure with Piezoresistive Detection Technique Using Coventorware FEA’, *Procedia Computer Science*, 93, pp. 146–152. doi:10.1016/j.procs.2016.07.194.

Nordström, M. *et al.* (2008) ‘SU-8 Cantilevers for Bio/chemical Sensing; Fabrication, Characterisation and Development of Novel Read-out Methods’, *Sensors*, 8(3), pp. 1595–1612. doi:10.3390/s8031595.

Rao, D.N. and Wootla, B. (2007) ‘Catalytic antibodies: Concept and promise’, *Resonance*, 12(11), pp. 6–21. doi:10.1007/s12045-007-0110-6.

Rosen, Y. and Gurman, P. (2010) ‘MEMS and Microfluidics for Diagnostics Devices’, *Current Pharmaceutical Biotechnology*, 11(4), pp. 366–375. doi:10.2174/138920110791233316.

Saylan, Y. *et al.* (2019) ‘An Alternative Medical Diagnosis Method: Biosensors for Virus Detection’, *Biosensors*, 9(2), p. 65. doi:10.3390/bios9020065.

Vasan, A.S.S., Doraiswami, R. and Pecht, M. (2011) ‘Embedded 3D BioMEMS for multiplexed label free detection’, in *2011 IEEE 61st Electronic Components and Technology Conference (ECTC)*. *2011 IEEE 61st Electronic Components and Technology Conference (ECTC)*, Lake Buena Vista, FL, USA: IEEE, pp. 1412–1419. doi:10.1109/ECTC.2011.5898697.

Vineetha, K.V. *et al.* (2018a) ‘Design of MEMS sensor for the detection of cholera and diarrehea by capacitance modulation’, *Microsystem Technologies*, 24(8), pp. 3371–3379. doi:10.1007/s00542-017-3702-4.

Wadas, M.J. *et al.* (2017) ‘Detection of Traumatic Brain Injury Protein Biomarkers With Resonant Microsystems’, *IEEE Sensors Letters*, 1(6), pp. 1–4. doi:10.1109/LSENS.2017.2768514.

Wee, K.W. *et al.* (2005) ‘Novel electrical detection of label-free disease marker proteins using piezoresistive self-sensing micro-cantilevers’, *Biosensors and Bioelectronics*, 20(10), pp. 1932–1938. doi:10.1016/j.bios.2004.09.023.

Yanagida, Y. (2017) ‘MEMS/NEMS-based Devices for Bio-measurements’, *Electrochemistry*, 85(9), pp. 572–579. doi:10.5796/electrochemistry.85.572.

Yang, J. *et al.* (2016) ‘Piezoresistive Silicon Cantilever Covered by ZnO Nanorods for Humidity Sensing’, *Procedia Engineering*, 168, pp. 1114–1117. doi:10.1016/j.proeng.2016.11.361.

Yu-Jie Huang *et al.* (2013) 'A CMOS Cantilever-Based Label-Free DNA SoC With Improved Sensitivity for Hepatitis B Virus Detection', *IEEE Transactions on Biomedical Circuits and Systems*, 7(6), pp. 820–831. doi:10.1109/TBCAS.2013.2247761.

Zhou, Y. *et al.* (2009) 'Design, fabrication and characterization of a two-step released silicon dioxide piezoresistive microcantilever immunosensor', *Journal of Micromechanics and Microengineering*, 19(6), p. 065026. doi:10.1088/0960-1317/19/6/065026.

Loui, A., Goericke, F.T., Ratto, T.V., Lee, J., Hart, B.R. and King, W.P., (2008) 'The effect of piezoresistive microcantilever geometry on cantilever sensitivity during surface stress chemical sensing'. *Sensors and Actuators A: Physical*, *147*(2), pp.516-521.

Lee, J.A. and Verleysen, M., (2007). *Nonlinear dimensionality reduction* (Vol. 1). New York: Springer.

Submitted: 12/05/2022
Revised: 21/06/2022
Accepted: 23/06/2022
DOI : 10.48129/kjs.20495